Large impact of the weak direct photoionization on the angularly resolved CO+(A2) de-excitation spectra of the CO*(112) resonance

Ph V Demekhin, I D Petrov, T Tanaka, M Hoshino, H Tanaka, K Ueda, W Kielich, A Ehresmann

Large impact of the weak direct photoionization on angularly resolved $CO^+(A\ ^2\Pi)$ de-excitation spectra of the $CO^*(1\sigma^{-1}2\pi)$ resonance

Ph V Demekhin[1], I D Petrov[2], T Tanaka[3], M Hoshino[3], H Tanaka[3], K Ueda[4], W Kielich[1], and A Ehresmann[1]

[1] Institute of Physics and CINSaT, University of Kassel, D-34132 Kassel, Germany

[2] Rostov State University of Transport Communications, 344038 Rostov-on-Don, Russia

[3] Department of Physics, Sophia University, Tokyo 102-8554, Japan

[4] Institute of Multidisciplinary Research for Advanced Materials, Tohoku University, Sendai 980-8577, Japan

E-mail: demekhin@physik.uni-kassel.de; ueda@tagen.tohoku.ac.jp

Abstract. Interference between the direct and resonant amplitudes for the population of the $CO^+(A\ ^2\Pi)$ state in the vicinity of the O 1s $\rightarrow 2\pi$ excitation of CO^* is studied by an *ab initio* theoretical approach. The weak direct photoionization induces Fano-Shore type profiles resulting in long-range exciting-photon energy dependencies of the computed angular distribution parameters for the $CO^+(A\ ^2\Pi)$ photoelectrons, $\beta_A^e(\omega)$, and for the subsequent $CO^+\left(A\ ^2\Pi \rightarrow X\ ^2\Sigma^+\right)$ fluorescence, $\beta 2_A^X(\omega)$. In the presence of the direct photoionization, the lifetime vibrational interference causes substantial variations of the computed parameter $\beta_A^e(\omega)$ across the positions of the $CO^*(v_r)$ vibronic states. Theoretical results are in qualitative agreement with the vibrationally and angularly resolved $CO^+(A\ ^2\Pi)$ resonant Auger electron spectra recorded in the Raman regime at different exciting-photon energies across the CO^* resonance.

PACS numbers: 33.80.-b, 32.80.Hd, 33.50.Dq

1. Introduction

The resonant Auger (RA) effect of core-excited simple molecules is a widely used prototype to study quantum mechanical interference effects [1]. Vibronic states of the core-excited molecule are broadened by their natural Auger decay lifetime. If the lifetime widths of these states are comparable with, or larger than, their vibrational spacings, the vibronic core-excited states overlap, and the lifetime vibrational interference (LVI) [2] takes place. Clear fingerprints of the LVI were unambiguously identified in the O 1s $\rightarrow 2\pi$ RA electron and subsequent fluorescence emission spectra for the O_2^*, NO^*, and CO^* molecules [3, 4, 5, 6, 7].

In the vicinity of the core-excitations of these molecules, the resonant photoionization channel dominates over the direct non-resonant population of the final states for the RA decay. As demonstrated in the detailed study of the O 1s $\rightarrow 2\pi$ excitation of CO^* [7], the LVI is the dominant effect in the on-resonance excitation regime. In the off-resonance excitation regime, the interference between the weak direct and resonant photoionization channels starts to play an important role [8, 9, 10]. In [9], quenching and restoring of the vibrational intensity distributions in the $CO^+(A\ ^2\Pi)$ Auger electron spectra were observed by the exciting-photon energy detunings below the $v_r = 0$ vibrational level of the $CO^*(1\sigma^{-1}2\pi)$ resonance. These effects were interpreted in [9] in terms of a Fano destructive interference between the direct and resonant photoionization channels by model simulations involving parametrization of the resonant and direct electronic transition amplitudes.

In our recent study of the RA decay of the $C^*O(2\sigma^{-1}2\pi)$ resonance [10] it was demonstrated that the weak direct photoionization plays an important role in describing the angularly resolved spectra, resulting in broad exciting-photon energy dependencies of the Auger electron and subsequent molecular fluorescence angular distribution parameters. The main goal of the present work is to study the influence of the direct photoionization on the angularly resolved $CO^+(A\ ^2\Pi)$ RA electron and subsequent $CO^+\,(A\ ^2\Pi \rightarrow X\ ^2\Sigma^+)$ fluorescence spectra in the vicinity of the

$CO^*(1\sigma^{-1}2\pi)$ resonance. For this purpose we apply the previously developed *ab initio* theoretical approach [10], outlined in section 2. Experimentally, we have recorded the angularly and vibrationally resolved $CO^+(A\ ^2\Pi)$ RA electron spectra. Details of the present experiment are summarized in section 3. Theoretical and experimental results are compared and discussed in section 4. We conclude with a brief summary.

2. Theory

The processes relevant to the present study can be schematically represented as follows:

$$\begin{array}{ll} (G) & \mathrm{CO} \quad 1\sigma^2 1\pi^4 5\sigma^2\,(X\ ^1\Sigma^+, v_0 = 0) + \hbar\omega \\ & \downarrow \quad \textit{Resonant core excitation} \\ (R) & \mathrm{CO}^* \ 1\sigma^1 1\pi^4 5\sigma^2 2\pi^1\,(^1\Pi, v_r) \\ & \Downarrow \quad \textit{Autoionization / Direct ionization} \\ (D) & \mathrm{CO}^+ \ 1\sigma^2 1\pi^3 5\sigma^2\,(A\ ^2\Pi, v') + \varepsilon\ell m\mu \\ & \downarrow \quad \textit{Fluorescence decay} \\ (F) & \mathrm{CO}^+ \ 1\sigma^2 1\pi^4 5\sigma^1\,(X\ ^2\Sigma^+, v'') + \varepsilon\ell m\mu + hc/\lambda \end{array} \tag{1}$$

Linearly polarized synchrotron radiation with an energy ω of around 533.42 eV (adiabatic $0-0$ transition [9]) excites the ground state of the CO molecule (G) into the $1\sigma^{-1}2\pi, v_r$ vibronic resonances of the CO^* molecule (R) with their subsequent autoionization via a participator Auger decay into the $CO^+(A\ ^2\Pi, v')\,\varepsilon\ell m\mu$ continua (D). In addition, the direct population of the $CO^+(A\ ^2\Pi, v')$ ionic states via a $(G) \rightarrow (D)$ dipole transition takes place (not indicated in scheme (1) for brevity). Ionization of the 1π- electron results in emission of $\varepsilon\ell\sigma$-, $\varepsilon\ell\pi$-, or $\varepsilon\ell\delta$- photoelectrons. The intermediate $CO^*(1\sigma^{-1}2\pi\ ^1\Pi)$ resonance may autoionize, however, only into the $1\pi^3(^2\Pi)\varepsilon\ell\sigma\ ^1\Pi$ and $1\pi^3(^2\Pi)\varepsilon\ell\delta\ ^1\Pi$ channels, but not into the $1\pi^3(^2\Pi)\varepsilon\ell\pi\ ^1\Sigma^+$ one. Thus, if one neglects the spin-orbit interaction in the continuous spectrum and the couplings of electronic states due to the molecular rotational motion, the $\varepsilon\ell\sigma$- and $\varepsilon\ell\delta$- partial waves can be generated via both, the resonant and direct photoionization channels, whereas the $\varepsilon\ell\pi$-photoelectron can be produced only via direct photoionization. The $A\ ^2\Pi, v'$ states of

the CO^+ ion decay in the next step via emission of a photon in the visible fluorescence range ($\lambda = 300 - 700$ nm, [11]) into the $X\ ^2\Sigma^+, v''$ states (F).

The angular distribution of photoelectrons after excitation of randomly oriented diatomic molecules by linearly polarized light is given by the well known formula [12]:

$$\frac{\mathrm{d}\sigma_{\Omega_1 v_1}(\omega)}{\mathrm{d}\Omega} = \frac{\sigma_{\Omega_1 v_1}(\omega)}{4\pi}\left[1 + \beta^e_{\Omega_1 v_1}(\omega) P_2(\cos\theta)\right], \tag{2}$$

where θ is the angle between the electric field vector of the exciting radiation and the direction of propagation of the outgoing electron. In Hund's coupling case (a) or (b), the total photoionization cross section, $\sigma_{\Omega_1 v_1}(\omega)$, and the electron angular distribution parameter, $\beta^e_{\Omega_1 v_1}(\omega)$, entering equation (2) can be computed via [10, 12]:

$$\begin{aligned}\sigma_{\Omega_1 v_1}(\omega) &= \frac{4\pi^2 \alpha a_0^2 \omega}{3 g_{\Omega_0}} \sum_{\Omega_0 \Omega_1} \sum_{\ell m \mu k} |\langle \Omega_1 v_1, \varepsilon \ell m \mu | \mathbf{d}_k | \Omega_0 v_0 \rangle|^2 \\ &= \sum_{\Omega_0 \Omega_1} \sum_{\ell m} \sum_{\mu k} |D_k\left(\Omega_1 v_1, \varepsilon \ell m \mu\right)|^2, \end{aligned} \tag{3}$$

$$\begin{aligned}\beta^e_{\Omega_1 v_1}(\omega) = \frac{1}{\sigma_{\Omega_1 v_1}(\omega)} \sum_{\Omega_0 \Omega_1} \sum_{\ell m} \sum_{\ell' m'} \sum_{k k'} \sum_{\mu} (i)^{\ell + \ell'} \sqrt{30(2\ell+1)(2\ell'+1)} (-1)^{\ell' + m + k} \\ \times e^{-i(\delta_{\ell m} - \delta_{\ell' m'})} \begin{pmatrix} \ell & \ell' & 2 \\ 0 & 0 & 0 \end{pmatrix} \begin{pmatrix} \ell & \ell' & 2 \\ m & -m' & k' - k \end{pmatrix} \begin{pmatrix} 1 & 1 & 2 \\ -k & k' & k - k' \end{pmatrix} \\ \times D_k\left(\Omega_1 v_1, \varepsilon \ell m \mu\right) D^*_{k'}\left(\Omega_1 v_1, \varepsilon \ell' m' \mu\right), \end{aligned} \tag{4}$$

The following notations are used in equations (3) and (4): Ω is the projection of the total electronic angular momentum along the molecular axis, and is supposed to be a good quantum number for the electronic state; v is the vibrational quantum number; $\varepsilon \ell m \mu$ stands for a photoelectron in a continuous spectrum, which can be expanded in the asymptotical region via partial waves [12] with fixed projections m and μ of the orbital angular momentum ℓ and spin s on the molecular axis, and a given phase shift $\delta_{\ell m}$; $\alpha = 1/137.036$ is the fine structure constant; the square of the Bohr radius $a_0^2 = 28.0028$ Mb converts atomic units for cross sections into megabarn (1 Mb $= 10^{-22}$ m^2); g_{Ω_0} is the statistical weight of the initial electronic state $|\Omega_0\rangle$; and the energy ω is connected with the energy of the photoelectron, ε, and the energy of the $|\Omega_1 v_1\rangle$ ionic state, $E_{\Omega_1 v_1}$, as: $\omega = E_{\Omega_1 v_1} + \varepsilon$.

For randomly oriented diatomic molecules excited by linearly polarized light, the angular distribution of fluorescence emitted via the subsequent $|\Omega_1 v_1\rangle \rightarrow |\Omega_2 v_2\rangle$ transition is given by [10]:

$$\frac{\mathrm{d}I^{\Omega_2 v_2}_{\Omega_1 v_1}(\omega)}{\mathrm{d}\Omega} = \frac{I^{\Omega_2 v_2}_{\Omega_1 v_1}(\omega)}{4\pi}\left[1 + \beta 2^{\Omega_2 v_2}_{\Omega_1 v_1}(\omega) P_2(\cos\theta)\right], \tag{5}$$

where θ is the angle between the electric field vector of the exciting radiation and the direction of detection of the fluorescence radiation. Here, the total fluorescence intensity, $I^{\Omega_2 v_2}_{\Omega_1 v_1}(\omega)$, is a product of the total cross section (3) and the fluorescence yield, $\chi^{\Omega_2 v_2}_{\Omega_1 v_1}$:

$$I^{\Omega_2 v_2}_{\Omega_1 v_1}(\omega) = \sigma_{\Omega_1 v_1}(\omega)\, \chi^{\Omega_2 v_2}_{\Omega_1 v_1}, \tag{6}$$

The equation for the fluorescence angular distribution parameter, $\beta 2^{\Omega_2 v_2}_{\Omega_1 v_1}(\omega)$, derived in our previous work [10] for the general case and simplified for the case of the CO^+ ($A\ ^2\Pi \rightarrow X\ ^2\Sigma^+$) fluorescence reads:

$$\beta 2^{X\Omega_2 v_2}_{A\Omega_1 v_1}(\omega) = \frac{-\frac{1}{10}\sigma^{\varepsilon\sigma}_{A\Omega_1 v_1}(\omega) + \frac{1}{5}\sigma^{\varepsilon\pi}_{A\Omega_1 v_1}(\omega) - \frac{1}{10}\sigma^{\varepsilon\delta}_{A\Omega_1 v_1}(\omega)}{\sigma_{A\Omega_1 v_1}(\omega)}, \tag{7}$$

where the kinematics coefficients are the same for the $|\Omega_1 = \pm\frac{1}{2}\rangle$ and $|\Omega_1 = \pm\frac{3}{2}\rangle$ initial fluorescence states, which are non-degenerate owing to the spin-orbit interaction of the 1π-electron. According to equation (7), $\beta 2^X_A$ is given by the incoherent sum of the partial photoionization cross sections, $\sigma^{\varepsilon\lambda}_{A\Omega_1 v_1}(\omega)$, corresponding to the emission of the $\varepsilon\sigma$-, $\varepsilon\pi$-, or $\varepsilon\delta$- photoelectrons. Since the value of the parameter (7) is independent of the transition amplitudes for the radiative decay into the $X\ ^2\Sigma^+(v'')$ states, and, therefore, of the vibrational quantum number v'', one obtains similar angular distributions for all fluorescence bands within the $A\ ^2\Pi(v' = const) \rightarrow X\ ^2\Sigma^+(v'')$ vibrational progression.

The partial transition amplitude for the population of the $|\Omega_1 v_1\rangle$ vibronic state from the initial state $|\Omega_0 v_0\rangle$ of a molecule in the vicinity of the $|\Omega_r v_r\rangle$ resonances is given by the coherent sum of the direct and different resonant amplitudes [10]:

$$D_k\left(\Omega_1 v_1, \varepsilon\ell m\mu\right) =$$
$$\sqrt{\frac{4\pi^2\alpha a_0^2\omega}{3g_{\Omega_0}}}\left\{\langle\Omega_1 v_1, \varepsilon\ell m\mu|\mathbf{d}_k|\Omega_0 v_0\rangle + \sum_{\Omega_r v_r}\frac{\langle\Omega_1 v_1, \varepsilon\ell m\mu|\frac{1}{|\mathbf{r}_{12}|}|\Omega_r v_r\rangle\langle\Omega_r v_r|\mathbf{d}_k|\Omega_0 v_0\rangle}{\omega - E_{\Omega_r v_r} + \frac{i}{2}\Gamma_{\Omega_r}}\right\}, \tag{8}$$

where $E_{\Omega_r v_r}$ are the energies of the vibronic resonances $|\Omega_r v_r\rangle$, and their natural widths, Γ_{Ω_r}, are assumed to be independent of the quantum number v_r. The

transition amplitudes (8) were computed in the present work within the Franck-Condon approximation. The electronic matrix elements were computed at the equilibrium internuclear distance of the ground state of CO, $r_e = 2.13$ a.u [13]. In the calculations of the transition amplitudes (8) relaxation (monopole rearrangement) of the molecular core was taken into account similar to our previous study of the C*O resonance [10].

For the $X\ ^1\Sigma^+$ ground state of the CO molecule and for the $X\ ^2\Sigma^+$ and $A\ ^2\Pi$ states of the CO^+ ion we utilized the *ab initio* potential energy curves computed in our previous work [10]. The potential energy curve of the $1\sigma^{-1}2\pi\ ^1\Pi$ core-excited state of the CO^* molecule was computed by applying the equivalent core '$Z+1$' approximation similar to our previous studies of the core-excited states of the N_2, NO, and CO molecules [5, 10, 14]. Thus, we computed the potential curve for the $X\ ^2\Pi$ ground state of the CF molecule by applying the Multi Reference Configuration Interaction (MRCI) approach. The energy of the zero vibrational level, $E_{v_r=0}$, of the computed curve was set to the experimental energy of 533.42 eV [9]. In order to eliminate a small inaccuracy of the '$Z+1$' approximation we used the experimental total ion yield spectrum from [7]. A good agreement between vibrational intensity distributions in the computed and measured total ion yield spectra was obtained by applying a small shift to the equilibrium internuclear distance, $\Delta r_e = +0.03$ a.u., of the computed potential curve.

The occupied molecular orbitals of the CO molecule were computed within the MO LCAO approach, whereas the single center (SC) method [10, 15, 16] with precise molecular field potentials was applied in order to compute partial waves for the photoelectron in the continuous spectrum. According to the SC method the molecular orbital (MO) of a diatomic molecule (where the projection m of the angular momentum ℓ along the internuclear axis is conserved) is represented as an expansion by spherical harmonics, $Y_{\ell m}(\theta,\varphi)$, with respect to the center (midpoint between the two nuclei):

$$\Psi_{nm}(x,y,z) = \sum_{\ell} \frac{P_{n\ell m}(r)}{r} Y_{\ell m}(\theta,\varphi), \tag{9}$$

where r,θ,φ are the coordinates with respect to the center, $P_{n\ell m}(r)$ stands for the radial parts of the partial harmonics in the SC expansion of the MO. The radial parts $P_{n\ell m}(r)$

of the photoelectron molecular orbital satisfy the following system of coupled differential Hartree-Fock equations [10, 15, 16]:

$$\sum_{\ell'}\left[\left(-\frac{\mathrm{d}^2}{\mathrm{d}r^2}+\frac{\ell(\ell+1)}{r^2}-\varepsilon_{nm}\right)\delta_{\ell\ell'}+V^{ne}_{\ell\ell'}(r)+V^{ee}_{\ell\ell'}(r)\right]P_{n\ell' m}(r)=0. \tag{10}$$

In the system of equations (10) the following designations are used: ε_{nm} is the one-electron energy measured in Rydberg units, $V^{ne}_{\ell\ell'}(r)$ is the potential describing nuclear-electron interaction, and $V^{ee}_{\ell\ell'}(r)$ is the potential describing direct and exchange electrostatic Coulomb interactions of the photoelectron with the ionic core. These potentials were calculated using the LCAO MOs of the occupied shells deconvolved as (9). The method for numerically solving the system of integro-differential equations (10) in the continuous spectrum ($\varepsilon_{nm} > 0$), resulting in observable incoming partial photoelectron waves normalized on the energy scale and satisfying the condition of mutual orthogonality, is described in detail in [10, 15].

3. Experiment

The present experiment is quite similar to that performed in [7, 9], therefore only its essentials relevant for obtaining the angularly resolved spectra are outlined below. It was carried out using linearly polarized synchrotron radiation from the high-resolution photochemistry beamline 27SU at SPring-8 in Japan. The polarization vector $\mathcal{E}$ of the undulator light may be set to horizontal (first harmonic) or vertical (0.5th harmonic) at this beamline [17]. The spectra were measured using the high-resolution electron-energy analyzer (Gammadata Scienta SES-2002). The lens axis was in the horizontal direction, at right angles to the photon beam direction, thus, the electron spectra recorded with horizontal and vertical polarization correspond to the electron emission parallel and perpendicular to the $\mathcal{E}$ vector, respectively. All spectra were normalized to the data acquisition time, the gas pressure, and the photon flux.

The degree of linear polarization of the synchrotron radiation was found to be larger than 0.98 for the current optical settings [7, 9]. Under these conditions, the

angular distribution parameter for the RA electrons can be obtained from the 0° and 90° spectra measured at the same exciting-photon energy according to:

$$\beta^e = 2\,\frac{I(0°) - I(90°)}{I(0°) + 2I(90°)}. \tag{11}$$

The monochromator bandpass was set to 67 meV FWHM, the electron spectrometer bandpass to 63 meV, resulting together with the Doppler broadening of around 54 meV in a total experimental linewidth for the electron spectra of around 107 meV. Electron spectra were recorded in the vicinity of the O 1s $\rightarrow 2\pi$ excitation of CO^* at different energies. The exciting-photon energy calibration was made by measuring the total ion yield and comparing to published absorption spectra [18]. The accuracy in the exciting-photon energy determination is found to be around ± 40 meV.

In order to determine the electron angular distribution parameters, intensities of the RA electron spectra measured at 0° and 90° were fitted at each exciting-photon energy. Parameters β^e were determined from the fitting results via relation (11). Uncertainties in determining the β^e values include statistical experimental dispersions, uncertainties due to subtraction of the background noise from the measured RA spectra, as well as fitting procedure errors. The present experimental results are discussed in subsection 4.2.

4. Results and discussion

4.1. Resonant Auger spectra

The accuracy of the present theoretical approach was checked by computing the participator Auger spectra of the CO^* resonance into the $CO^+(A\ ^2\Pi)$ state. The RA electron spectra computed in the present work and measured in [7] at the exciting-photon energies 533.90, 534.20, and 534.62 eV, corresponding to excitation of the $v_r = 3$, 5, and 8 vibrational levels of the $CO^*(1\sigma^{-1}2\pi)$ resonance, are compared in Fig. 1. The figure illustrates very good agreement between vibrational intensity distributions in the computed and measured spectra. The latter fact allows us to

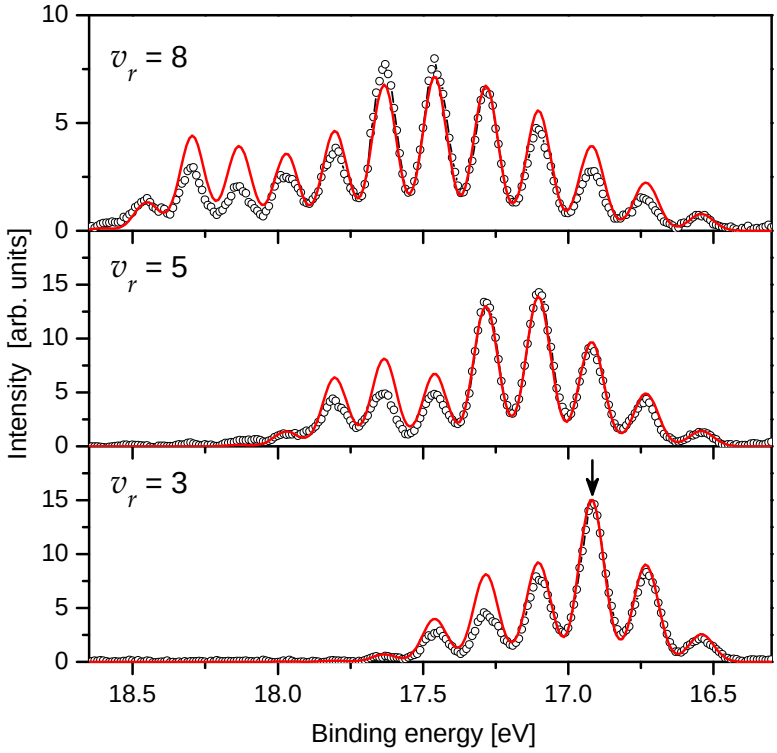

Figure 1. (Color online) Presently computed (solid curves) and measured in [7] (open circles) normalized RA electron spectra for the $CO^+(A\ ^2\Pi)$ state corresponding to excitations of the $v_r = 3$, 5, and 8 vibrational levels of the $CO^*(1\sigma^{-1}2\pi)$ resonance. The theoretical intensities are equalized with the experimental ones in the point indicated by the vertical arrow in the lowest panel.

conclude that our calculations accurately reproduce the LVI in the resonant population of the $CO^+(A\ ^2\Pi, v')$ vibronic states, which is known to be the dominant effect in the on-resonance excitation regime [7].

As follows from the detailed study of the O 1s $\rightarrow 2\pi$ excitation of CO^* [9], in the off-resonance excitation regime, the Fano destructive interference between the direct and resonant photoionization amplitudes plays an important role in formation of the $CO^+(A\ ^2\Pi)$ RA electron spectra. The presently computed RA electron spectra for the exciting-photon energy detunings below the $v_r = 0$ vibrational level (533.42 eV) of the $CO^*(1\sigma^{-1}2\pi)$ resonance are compared with the experimental [9] ones in Fig. 2. We note, that the computed vibrational intensity distributions in the electron spectra depicted in

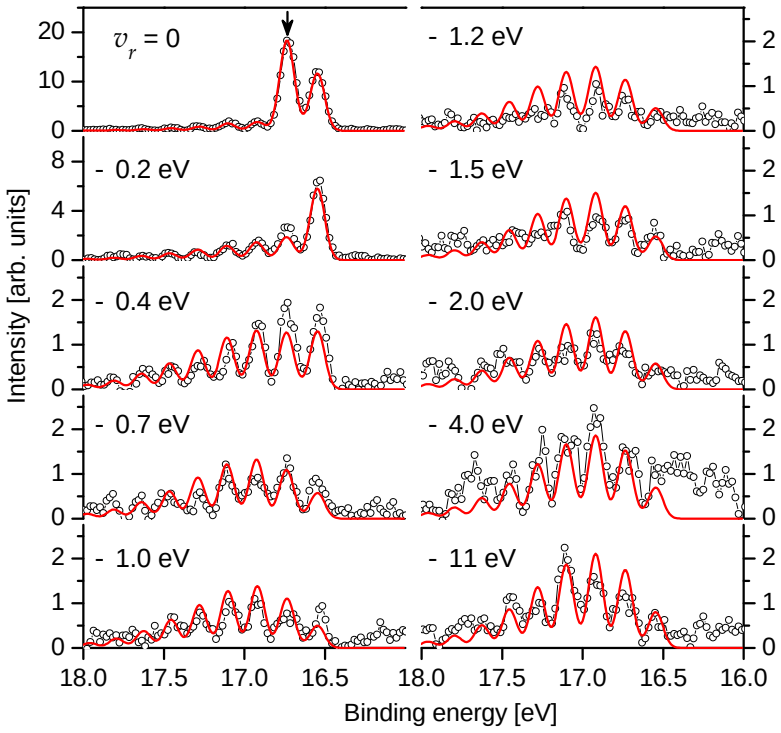

Figure 2. (Color online) Presently computed (solid curves) and measured in [9] (open circles) normalized RA electron spectra for the $CO^+(A\ ^2\Pi)$ state corresponding to exciting-photon energy detunings (indicated in each panel) below the $v_r = 0$ vibrational level of the $CO^*(1\sigma^{-1}2\pi)$ resonance. The theoretical intensities are equalized with the experimental ones in the point indicated by the vertical arrow in the uppermost left panel.

Fig. 2 agrees with the measured intensity distributions considerably better than those, simulated in [9]. Especially in the detuning energy range between -0.4 and -2.0 eV, where simulations from [9] yield a lack of intensity due to a completely destructive interference between the direct and resonant photoionization channels (see discussion related with Figs. 2 and 3 in [9]). This is due to the fact, that the direct photoionization was represented in [9] by only one channel (amplitude).

More detailed conclusions on the destructive interference between the direct and resonant amplitudes can be drawn from Fig. 3, where the presently computed total and partial cross sections for the population of the $CO^+(A\ ^2\Pi, v' = 0)$ vibronic state are depicted in the vicinity of the minimum in enlarged scale. Strong destructive Fano

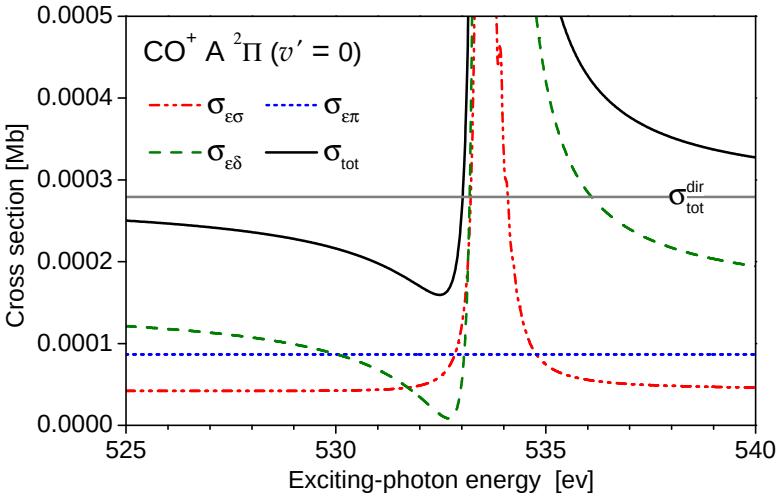

Figure 3. (Color online) Total and partial cross sections for the population of the $CO^+(A\ ^2\Pi, v'=0)$ vibronic state computed in the vicinity of the O 1s $\rightarrow 2\pi$ excitation of CO^*.

interference in the most probable $\varepsilon\delta$- photoionization channel is obvious from this figure (cross section nearly vanishes in its minimum). In the $\varepsilon\sigma$- photoionization channel, the interference is rather weak resulting in a practically symmetric peak feature. As mentioned above, due to the symmetry selection rules the $\varepsilon\pi$- channel is purely non-resonant. Thus, the considered process represents the case of interaction of many resonances with many continua [19] with the parameter $\rho^2 \neq 1$. As a result, the total cross section for the population of the $CO^+(A\ ^2\Pi, v'=0)$ vibronic state (solid curve in Fig. 3) falls in its minimum only by about a half of its asymptotical value corresponding to the direct total photoionization cross section (horizontal solid line in Fig. 3). The same holds for the population of the other $CO^+(A\ ^2\Pi, v')$ vibronic states. That is why the presently computed intensities of the RA electron spectra in the detuning energy range between -0.4 and -2.0 eV do not vanish as in the simulations of [9].

4.2. Photoelectron angular distribution

Results of the present calculations for the first five vibronic states CO^+ $A\ ^2\Pi(v'=0-4)$ are summarized in Figs. 4–8, respectively. Calculations were performed within several

approximations:

- '*Direct*' – the direct transition amplitudes only were accounted for;
- '*LVI*' / '*2ST*' – the resonant photoionization amplitudes only were accounted for coherently;
- '*Interference*' – interference between the direct and resonant amplitudes was taken into account.

We note here that, if one neglects the direct photoionization, the computed angular distribution parameters become independent of the exciting-photon energy even though the nuclear vibrational motion and LVI are included. Indeed, within the Franck-Condon approximation and in absence of the direct photoionization amplitudes, the complete vibrational part of the transition amplitude (8) cancels in the numerators and denominators of equations (4) and (7). As a result, the computed values of the angular distribution parameters are determined only by the electronic part of the resonant transition amplitude, which is the same for all intermediate v_r and final v' vibrational states. The latter approximation in computing β^e and $\beta 2$ parameters is usually referred to as the two-step (2ST) model.

From Figs. 4–8 one can see that the resonant photoionization dominates over the direct one in the vicinity of the CO^* resonance (cf dashed horizontal lines and dash-dot-dotted curves in panels (a)). As discussed in the previous subsection, the destructive interference between dominant resonant and weak direct transition amplitudes on the low energy side forms minima in the photoionization cross sections. On the high energy side, computed cross sections are considerably increased with respect to the purely resonant population due to the constructive interference (cf dash-dot-dotted and solid curves in panels (a)).

The parameters $\beta^e_{Av'}(\omega)$ computed within the '*Direct*' approximation are practically constant in the vicinity of the resonance, since the direct amplitude varies only slightly in this energy interval. They are equal in the present case to 0.90 (dashed horizontal lines in panels (b)). As mentioned above, if one neglects the direct transition amplitudes, the

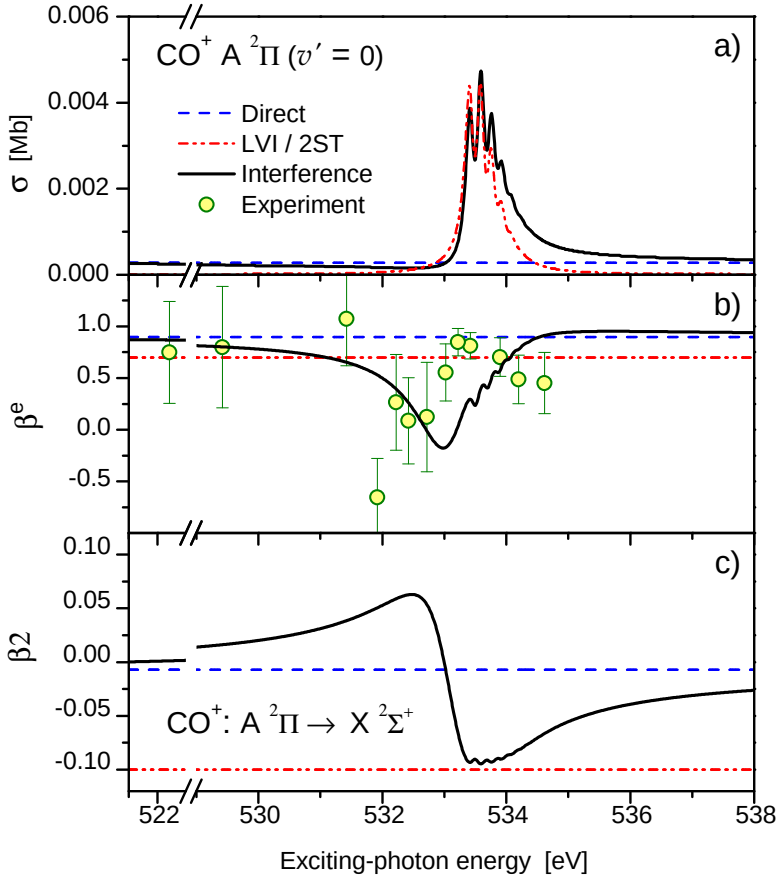

Figure 4. (Color online) Panel (a): Cross section for the population of the CO^+ $A\ ^2\Pi(v'=0)$ vibronic state in the vicinity of the CO^* resonance. Panel (b): Angular distribution parameter for the CO^+ $A\ ^2\Pi(v'=0)$ photoelectrons. Panel (c): Angular distribution parameter for the $A\ ^2\Pi(v'=0) \rightarrow X\ ^2\Sigma^+(v'')$ fluorescence bands progression. Note the abscissa axis break on the low energy side.

2ST model may be applied for the interpretation of the RA decay, yielding in our case the constant value 0.70 of the angular distribution parameter (dash-dot-dotted horizontal lines in panels (b)). Being included in the calculations, the interference between the direct and resonant amplitudes gives rise to the exciting-photon energy dependencies of the computed angular distribution parameters (solid curves in panels (b)). One can see that the interference influences the computed $\beta^e_{Av'}(\omega)$ far away from the resonance, and the corresponding resonant profiles in the $\beta^e_{Av'}(\omega)$ are much broader than in the $\sigma_{Av'}(\omega)$ [10].

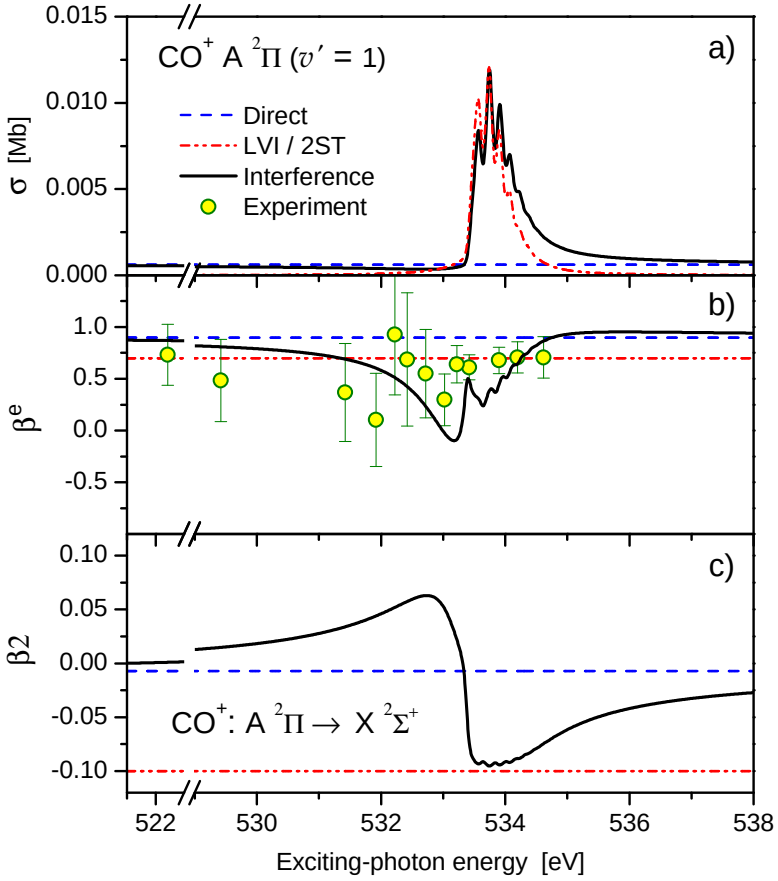

Figure 5. (Color online) Parameters computed and measured for the CO^+ $A\ ^2\Pi$ ($v' = 1$) state (see notations in Figure 4).

From Figs. 4–8 one can see that vibrational structures of the electronic states involved in the RA decay result in substantial variations of the computed parameters $\beta^e_{Av'}(\omega)$. The shape of the above variations is determined not only by the absolute value (like intensities of RA electron spectra), but also by the sign of the product of the two Franck-Condon factors corresponding to the excitation and subsequent Auger decay of the resonance, $\langle v'|v_r\rangle \cdot \langle v_r|v_0\rangle$. Extended investigations showed that in the present case, distinct variations correspond to a sign reversal of the $\langle v'|v_r\rangle$ factors only, because $\langle v_r|v_0\rangle > 0$. Since the photoionization cross sections enter equation (4) in the denominator, these variations are more pronounced in the region of the minimum in the $\sigma_{Av'}(\omega)$. We note again, that the fingerprints of the nuclear vibrational motion in the computed $\beta^e_{Av'}(\omega)$ parameters show up only due to the presence of the weak direct

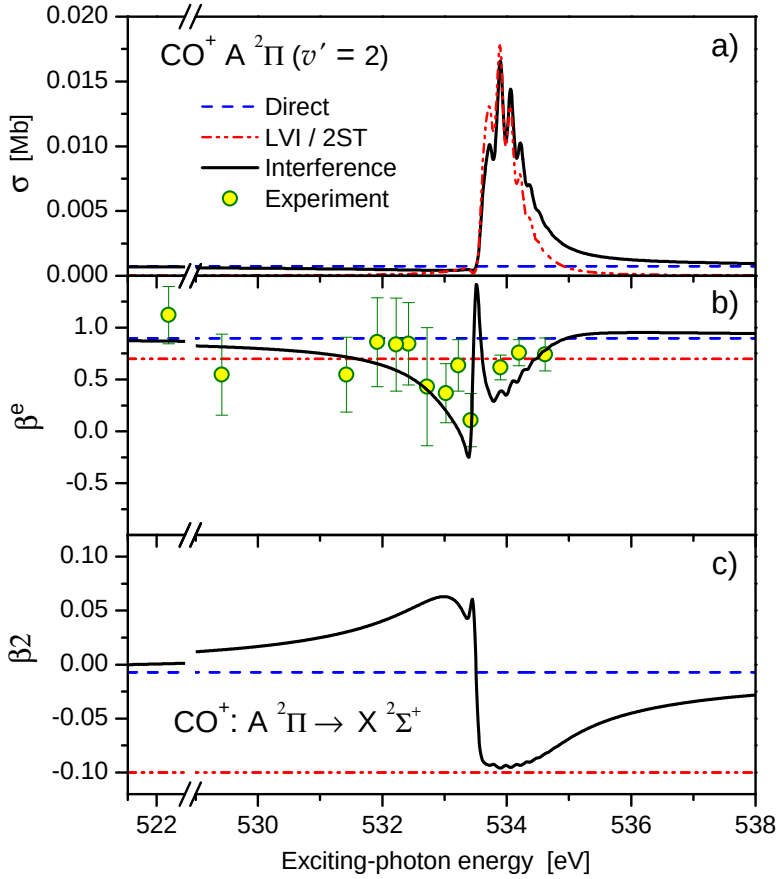

Figure 6. (Color online) Parameters computed and measured for the CO^+ A $^2\Pi$ ($v' = 2$) state (see notations in Figure 4).

photoionization.

The angular distribution parameters $\beta^e_{Av'}(\omega)$ measured in the present work at different exciting-photon energies are compared with the theoretical ones in panels (b) of Figs. 4–8 (open circles with error bars). In the off-resonance excitation regime, the fitting procedure was very sensitive to the multi-peak fitting parameters resulting in large experimental error bars, especially in the region of minima in the $\sigma_{Av'}(\omega)$. The figures illustrate an overall agreement between the absolute values of the measured and computed $\beta^e_{Av'}(\omega)$ parameters. The average curvatures of the measured and computed parameters have similar tendency. The experimental $\beta^e_{Av'}(\omega)$ parameters possess also variations across the resonance, supporting qualitatively the impact of the nuclear vibrational motion and direct photoionization illustrated by theory. A quantitative

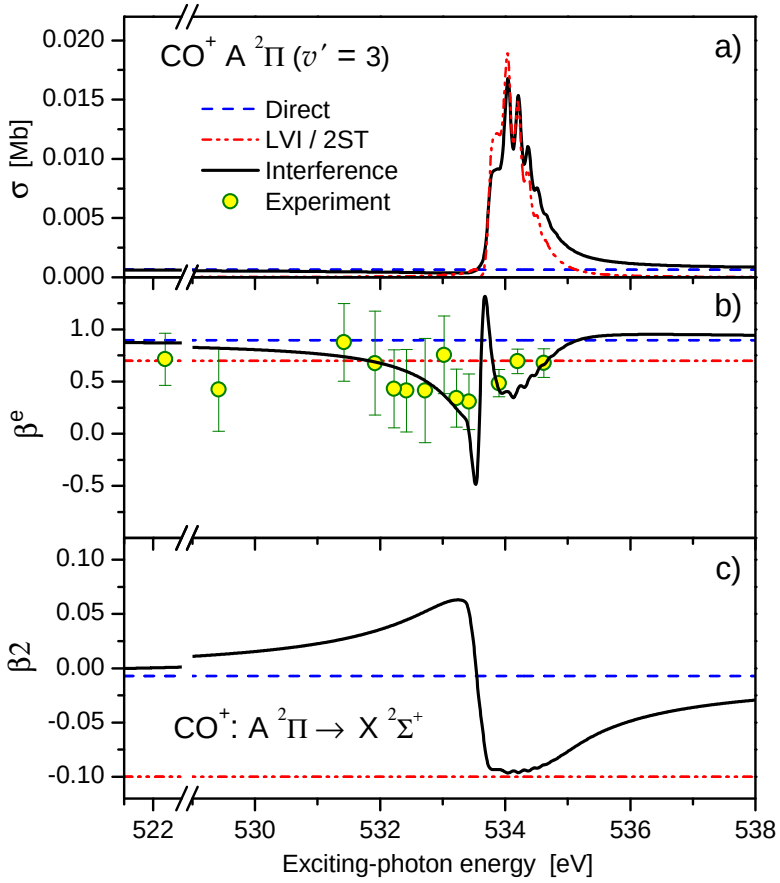

Figure 7. (Color online) Parameters computed and measured for the CO^+ $A\ ^2\Pi$ ($v' = 3$) state (see notations in Figure 4).

verification of the predicted effects would require considerable improvement of the experimental count rate (signal-to-noise ratio), especially in the energy detunings region.

The photoelectron angular distribution parameter (4) is given by the interplay between partial photoionization amplitudes and is much more sensitive to the approximation made in the calculations than the total cross section (3). One can therefore not expect the computed angular distribution parameters to be as accurate as the cross sections. A more precise calculation of the angular distribution parameters would require (i) a step beyond the presently applied Franck-Condon approximation in computing the transition matrix elements; and (ii) accounting for non-monopole electron correlations neglected in the present calculations of the electronic transition amplitudes. In addition, high-energy multiply-excited molecular states may influence

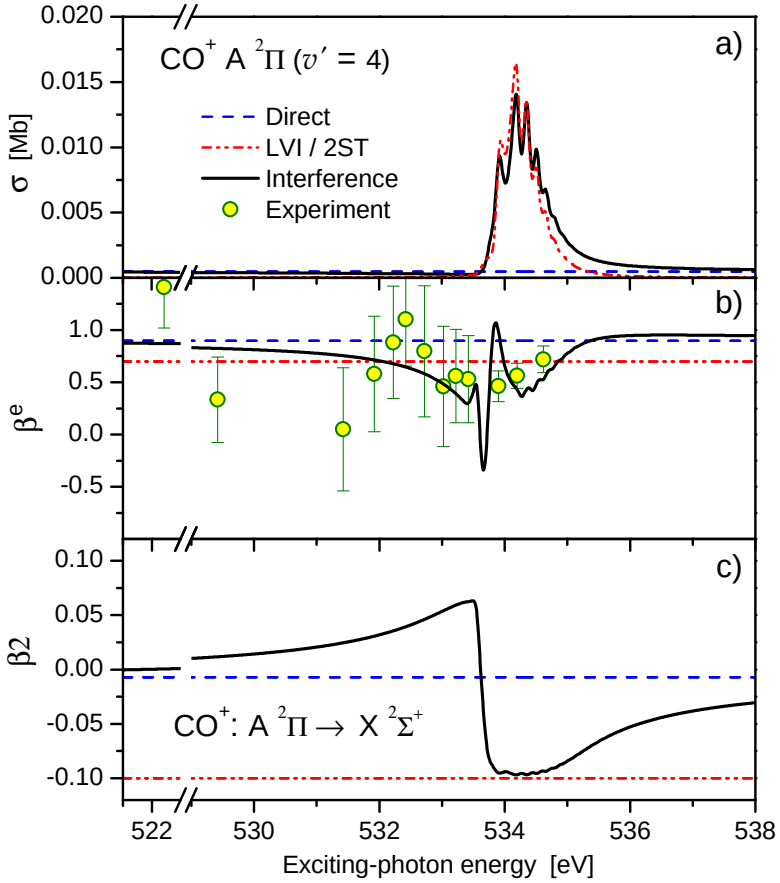

Figure 8. (Color online) Parameters computed and measured for the CO^+ $A\ ^2\Pi$ ($v' = 4$) state (see notations in Figure 4).

the angular distribution for RA electrons. These weakly populated states with many electrons excited from the core into unoccupied orbitals (one electron must be excited from the C 1s shell owing to energetic reasons) situated in the neighbourhood of the CO^* resonance may autoionize into the same continua. This could explain considerable leaps (larger than the present error bars) in the $\beta^e_{Av'}(\omega)$ functions observed in the off-resonance excitation regime: e.g., β^e_{A0}(531.92 eV), β^e_{A1}(531.92 eV), β^e_{A4}(522.42 eV), β^e_{A4}(529.42 eV), and β^e_{A4}(531.42 eV).

4.3. Fluorescence angular distribution

Theoretical predictions for the angular distribution parameters $\beta 2^{Xv''}_{Av'}(\omega)$ of the $A\ ^2\Pi(v') \rightarrow X\ ^2\Sigma^+(v'')$ fluorescence are shown in panels (c) of Figs. 4–8. Parameters

computed within the '*Direct*' approximation and '*2ST*' model are equal in the present case to -0.01 and -0.1, and are depicted by horizontal dashed and dash-dot-dotted lines, respectively. Interference between the direct and resonant amplitudes gives rise to the long-range asymmetric exciting-photon energy dependencies of the computed $\beta 2_{Av'}^{Xv''}(\omega)$ parameters across the $CO^*(1\sigma^{-1}2\pi)$ resonance (solid curves). In the on-resonance excitation regime, populations of the $A\ ^2\Pi(v')$ states are almost entirely determined by the $\varepsilon\sigma$- and $\varepsilon\delta$-channels, yielding according to equation (7) angular distribution parameters close to -0.1.

The opposite situation happens on the low energy side of the resonance, where the angular distribution parameters $\beta 2_{Av'}^{Xv''}(\omega)$ are positive. As demonstrated in Fig. 3 for the $v' = 0$ vibrational level, in the region of minimum in the total cross sections $\sigma_{Av'}(\omega)$, the purely non-resonant $\varepsilon\pi$- channel is more probable than both resonant $\varepsilon\sigma$- and $\varepsilon\delta$-ones. It has a positive kinematic coefficient $+0.2$, resulting in a small positive numerator of equation (7). In the region of the minimum in the total cross section $\sigma_{Av'}(\omega)$, the denominator of equation (7) becomes small, yielding a large positive value of the angular distribution parameter. As seen from panels (c) of Figs. 4–8, the computed $\beta 2_{Av'}^{Xv''}(\omega)$ parameters change their signs just in the minimum of the total photoionization cross section $\sigma_{Av'}(\omega)$.

5. Conclusions

We have computed the angular distribution parameters for the $CO^+(A\ ^2\Pi)$ photoelectrons and for the subsequent $CO^+(A\ ^2\Pi \rightarrow X\ ^2\Sigma^+)$ fluorescence in the vicinity of the O 1s $\rightarrow 2\pi$ excitation of CO^*. In the calculations, the interference between the weak direct and strong resonant photoionization channels was taken into account *ab initio*. The interference between many resonances and many continua results in the:

- low energy side Fano-Shore type minimum in the total cross section $\sigma_{Av'}(\omega)$ for the population of the $CO^+(A\ ^2\Pi, v')$ vibronic states, enabling a quantitative description of the energy detunings RA electron spectra measured in [9];

- long-range Fano-Shore profile type exciting-photon energy dependencies of the photoelectron and fluorescence angular distribution parameters $\beta^{e}_{Av'}(\omega)$ and $\beta 2^{Xv''}_{Av'}(\omega)$;
- distinct variations of the $\beta^{e}_{Av'}(\omega)$ parameters across the positions of the v_r vibrational levels, corresponding to the sign-reversal behavior of the Franck-Condon factors $\langle v'|v_r\rangle$ for the RA decay, enhanced by the minimum in the photoionization cross sections $\sigma_{Av'}(\omega)$;
- change of sign of the computed $\beta 2^{Xv''}_{Av'}(\omega)$ parameters in the vicinity of the minimum in the cross section function $\sigma_{Av'}(\omega)$.

In order to check the theoretical predictions, the angularly and vibrationally resolved CO^+ $A\ ^2\Pi$ (v') RA electron spectra were recorded in the vicinity of the O 1s $\rightarrow 2\pi$ excitation of CO^* at different exciting-photon energies corresponding to the on- and off- resonance excitation regimes. The experimental $\beta^{e}_{Av'}(\omega)$ parameters qualitatively agree with the computed ones, possessing similar average curvatures and distinct variations across the resonance as obtained in the calculations. However, relatively large experimental error bars do not allow us to unambiguously conclude on the quantitative agreement with the present theory. It would be very important to verify the change of sign of the $\beta 2^{Xv''}_{Av'}(\omega)$ parameters illustrated by the theory. For this purpose, the degree of polarization of the $CO^+(A\ ^2\Pi \rightarrow X\ ^2\Sigma^+)$ molecular fluorescence in the visible fluorescence range [11] (similar to the fluorescence angular distribution [10]) might be analyzed by means of fluorescence spectroscopy.

Acknowledgments

The authors would like to thank V. L. Sukhorukov for many valuable discussions and corrections of the manuscript. This work has been supported by the European Community's 7$^{\text{th}}$ Framework Programme (project no PIIF-GA-2008-219224), by the Deutsche Forschungsgemeinschaft (DFG) under contract no EH 187/16-1, and by the Bundesministerium für Bildung und Forschung (BMBF) FSP 301 (contract no

05KS7RK1). PhVD gratefully acknowledges the Marie Curie fellowship. IDP would like to thank the Institute of Physics, University of Kassel for the hospitality during his stay there. The experiment was carried out with the approval of the SPring-8 program review committee and partly supported by the Grants-in-Aid for Scientific Researches from the Japan Society for the Promotion of Science (JSPS).

References

[1] Gel'mukhanov F K and Ågren H 1999 *Phys. Rep.* **312** 87–330

[2] Gel'mukhanov F K, Mazalov L N and Kondratenko A V 1977 *Chem. Phys. Lett.* **46** 133–7

[3] Neeb M, Rubensson J-E, Biermann M and Eberhardt W 1994 *J. Electr. Spectr. Relat. Phenom.* **67** 261–74

[4] Wang H, Fink R F, Piancastelli M N, Bässler M, Hjelte I, Björneholm O, Burmeister F, Feifel R, Giertz A, Miron C, Sorensen S L, Wiesnera K and Svensson S 2003 *Chem. Phys.* **289** 31–44

[5] Ehresmann A, Kielich W, Werner L, Demekhin Ph V, Omel'yanenko D V, Sukhorukov V L, Schartner K-H and Schmoranzer H 2007 *Eur. Phys. J. D* **45** 235–46

[6] Piancastelli M N, Neeb M, Kivimäaki A, Kempgensy B, Köppe H M, Maier K, Bradshaw A M and Fink R F 1997 *J. Phys. B: At. Mol. Opt. Phys.* **30** 5677–92

[7] Tanaka T, Shindo H, Makochekanwa C, Kitajima M, Tanaka H, Fanis A D, Tamenori Y, Okada K, Feifel R, Sorensen S, Kukk E and Ueda K 2005 *Phys. Rev. A* **72** 022507(1–7)

[8] Carravetta V, Gelmukhanov F K, Ågren H, Sundin S, Osborne S J, Naves de Brito A, Björneholm O, Ausmees A and Svensson S 1997 *Phys. Rev. A* **56** 4665–74

[9] Feifel R, Tanaka T, Hoshino M, Tanaka H, Tamenori Y, Carravetta V and Ueda K 2006 *Phys. Rev. A* **74** 062717(1–6)

[10] Demekhin Ph V, Petrov I D, Sukhorukov V L, Kielich W, Reiss P, Hentges R, Haar I, Schmoranzer H and Ehresmann A 2009 *Phys. Rev. A* **80** 063425(1–12)

[11] Krupenie P H 1966 *Natl Std. Ref. Data Ser. Natl Bur. Std. (US)* **5** 1–87

[12] Cherepkov N A 1981 *J. Phys. B: At. Mol. Phys.* **14** 2165–77

[13] Huber K P and Herzberg G 1979 *Molecular Spectra and Molecular Structure. IV: Constants of Diatomic Molecules* (New York: Van Nostrand-Reinhold)

[14] Ehresmann A, Werner L, Klumpp S, Lucht S, Schmoranzer H, Mickat S, Schill R, Schartner K-H, Demekhin Ph V, Lemeshko M P and Sukhorukov V L 2006 *J. Phys. B: At. Mol. Opt. Phys.* **39** 283–304

[15] Demekhin Ph V, Omel'yanenko D V, Lagutinm B M, Sukhorukov V L, Werner L, Ehresmann A, Schartner K-H and Schmoranzer H 2007 *Optics and Spectroscopy* **102** 318–29

[16] Ehresmann A, Demekhin Ph V, Kielich W, Haar I, Schlüter M A, Sukhorukov V L and Schmoranzer H 2009 *J. Phys. B: At. Mol. Opt. Phys.* **42** 165103(1–10)

[17] Tanaka T and Kitamura H 1995 *Nucl. Instrum. Methods Phys. Res. A* **364** 368–73 ; 1996 *J. Synchrotron Radiat.* **3** 47–52

[18] Püttner R, Dominguez I, Morgan T J, Cisneros C, Fink R F, Rotenberg E, Warwick T, Domke M, Kaindl G and Schlachter A S 1999 *Phys. Rev. A* **59** 3415–23

[19] Shore B W 1968 *Phys. Rev.* **171** 43–54